



# An optimized Chlorophyll *a* switching algorithm for MERIS and OLCI in phytoplankton-dominated waters

M.E. Smith<sup>a,\*</sup>, L. Robertson Lain<sup>b</sup>, S. Bernard<sup>a</sup>

<sup>a</sup> NRE Earth Observation, CSIR, 15 Lower Hope Road, Rosebank, Cape Town 7700, South Africa

<sup>b</sup> Department of Oceanography, University of Cape Town, Rondebosch, 7700 Cape Town, South Africa

## ARTICLE INFO

### Keywords:

OLCI  
MERIS  
Chlorophyll *a*  
Southern Benguela

### MSC:

00-01  
99-00

## ABSTRACT

Productive upwelling zones such as the southern Benguela can exhibit phytoplankton biomass variability over several orders of magnitude, from near oligotrophic offshore waters to hypertrophic inshore blooms of  $> 100 \text{ mg m}^{-3}$ . This introduces complexity for ocean colour applications such as Harmful Algal Bloom (HAB) monitoring. As low and high biomass algorithmic approaches for ocean colour differ, no single algorithm can optimally retrieve accurate Chl *a* over such a wide range of biomass. We propose a novel technique to apply and blend two different Chl *a* algorithms — an empirical blue-green algorithm for low to moderate biomass and a red-NIR band-ratio algorithm for moderate to high biomass. The blending method is based on the 708 and 665 nm reflectance wavelength ratio, where the blue-green algorithm is applied when the  $\rho_w(708)/\rho_w(665)$  ratio is  $< 0.75$ , the red-NIR algorithm is applied  $> 1.15$ , whilst the two are blended using a weighted approach in between these values. When applied to *in situ* and satellite match-up data this method provides a median absolute relative difference (MARD) of 37.9 and 45.7%, respectively, and a RMSD of 0.27 and 0.35 respectively, over Chl *a* concentrations spanning three orders of magnitude. Application is demonstrated for both MERIS and OLCI sensors, providing a smooth transition between different biomass levels and algorithm Chl *a* returns.

## 1. Introduction

Deriving quantitative information of the biogeochemical constituents in the water column from satellite ocean colour data requires regionally or water type appropriate algorithms. As a component of all photosynthetic marine algae, Chlorophyll *a* concentration ([Chl *a*]) is often used as a proxy for phytoplankton biomass (O'Reilly et al., 1998).

Empirical algorithms that utilize relationships between reflectances in the blue and green spectral regions (e.g. O'Reilly et al., 1998; O'Reilly et al., 2000; Morel and Antoine, 2011) are often used to derive [Chl *a*] in open ocean or “Case 1” waters (Morel and Prieur, 1977; Gordon and Morel, 1983), where water constituents tend to covary with phytoplankton and its related degradation products. However, the assumptions that these algorithms are based upon can break down in productive or turbid waters (Dierssen, 2010). Algorithms utilizing the red-NIR part of the electromagnetic spectrum have often been preferred for ocean colour remote sensing of productive inland and coastal waters. This spectral region has several reflectance features that can be related to [Chl *a*], such as the height of the solar-induced Chl *a* fluorescence peak (e.g. Gower and King, 2007; Ryan et al., 2009), the reflectance peak around 700 nm which is often related to [Chl *a*] through

relationships with band ratio (Gitelson et al., 2011; Gurlin et al., 2011; Yacobi et al., 2011) and spectral band difference algorithms (Gower et al., 2005; Matthews et al., 2012).

Although both blue-green and red-NIR band ratio algorithms are mostly robust in their ability to provide coherent patterns of the synoptic phytoplankton biomass variability at their respective optimal [Chl *a*] ranges, the natural variation in IOPs often necessitate regional tuning to ensure lower uncertainty in [Chl *a*] retrievals (e.g. McKee et al., 2007; Volpe et al., 2007). To date there is no single algorithm that can provide accurate quantitative information across all water types.

To overcome this hurdle, specific thresholds or flags have been used to switch between different algorithms (e.g. Matsushita et al., 2015; Smith et al., 2013); however, these techniques run the risk of causing discontinuities that may not be apparent just by looking at the [Chl *a*] image, but which may show up with more detailed analysis (e.g. Hooker et al., 1995). More holistic methods have included fuzzy classification of reflectance spectra into predefined optical water types for application and blending of water type-appropriate algorithms (Moore et al., 2001, 2014); this method has now also been included as part of the ocean colour products produced by the ESA Climate Change Initiative to apply and blend class appropriate algorithms across merged

\* Corresponding author.

E-mail addresses: [msmith2@csir.co.za](mailto:msmith2@csir.co.za) (M.E. Smith), [sbernard@csir.co.za](mailto:sbernard@csir.co.za) (S. Bernard).

satellite datasets (Jackson et al., 2017). The Coast Colour project proposes a merged [Chl *a*] product, which blends the retrievals of a blue-green empirical algorithm and a neural network algorithm, based on the satellite retrieved concentration of total suspended matter (Brockmann, 2014). A similar method has been employed in the Yellow and East China Seas, where the height of the normalized water-leaving radiance at 555 nm was used to switch and blend between two regionally-modified algorithms for Case 1 and turbid waters, respectively (Siswanto et al., 2011). The novelty detection technique of D'Alimonte et al. (2003) uses the triplet of the logarithm of the  $R_{rs}$  at 490, 555, and 665 nm with a probability density function to blend the returns from two different neural network algorithms when satellite pixels are considered non-novel. Weighted algorithm switching and blending can also optimize retrievals in low biomass Case 1 environments; the NASA [Chl *a*] product, *chlora*, uses the colour index (CI) (Hu et al., 2012) and the standard OC3 for MODIS or OC4 for SeaWiFS (O'Reilly et al., 2000), whilst a transition between the two products occurs at CI values of 0.15 and 0.2 (Feldman and McClain, 2017). Kahru and Mitchell (2010) use both the maximum band ratio and the mean geographical position relative to the Subtropical Front to weight and blend their Southern Ocean specific algorithm with OC4, whilst Carder et al. (1999) blend semianalytical and empirical algorithms based on the phytoplankton absorption coefficient at 675 nm ( $a_p(675)$ ) value returned by the semianalytical algorithm. Weighted algorithm blending thus offers the ability to smoothly transition between water-type appropriate algorithms to ensure optimal retrievals and minimize spatial discontinuities.

The region of interest in the current study is the southern Benguela, a highly productive and dynamic eastern-boundary upwelling system. The optical conditions can be described as phytoplankton-dominated extreme Case 1 (Matthews et al., 2012), with inorganic particulates and coloured dissolved organics contributing very little to the bulk inherent optical properties. Due to the wind-driven and pulsed nature of the system, [Chl *a*] may range from approximately  $< 1$  to  $> 30 \text{ mg m}^{-3}$ , in newly and aged upwelled water respectively (Barlow, 1982), over a matter of days; [Chl *a*]  $> 100 \text{ mg m}^{-3}$  is often reported in bloom conditions (Pitcher and Nelson, 2006). Harmful algal blooms (HABs) occur frequently from January to May in the latter half of the upwelling season (Pitcher and Calder, 2000), which have the potential to negatively impact commercial and recreational activities in the region (Pitcher and Calder, 2000; Probyn et al., 2000). Although the [Chl *a*] product cannot directly describe the type of species or toxicity of a bloom, it can be used as an indicator for high biomass blooms that could potentially lead to hypoxic events (Pitcher and Weeks, 2006).

Whilst standard empirical algorithms may be sufficient to monitor the average coastal and offshore conditions of [Chl *a*]  $< 25 \text{ mg m}^{-3}$ , algorithms are also required to accurately assess the very high biomass ranges where potential harmful impacts from toxic diatom and toxic or hypoxia-causing dinoflagellate blooms may materialize. The water-leaving reflectance signal attributed to increasing phytoplankton biomass becomes dominated by features in the red part of the spectrum at around  $15 \text{ mg m}^{-3}$  (Robertson-Lain et al., 2014); thus, from a remote sensing perspective, operational monitoring of this highly variable system would benefit from a dynamic approach that utilizes appropriate algorithms corresponding to the dominant spectral features and *in situ* ranges of phytoplankton biomass, whilst providing optimal blended returns. We propose that it is possible to base an algorithm switch on the ratio of the reflectance peak near 700 nm, attributed to a combination of strong phytoplankton and water absorption and elevated phytoplankton backscattering, and the reflectance trough near 675 nm, caused by a maximum in Chl-*a* absorption. This ratio is strongly related to [Chl *a*] and is often employed in red-NIR algorithms (Gurlin et al., 2011).

In order to optimize this approach for satellite application, the 708 and 665 nm bands were utilized respectively. With the availability of good spectral coverage in the red-NIR the Level 2 radiometric data from both the Medium Resolution Imaging Spectrometer (MERIS) and the

Ocean and Land Colour Imager (OLCI) provide the ideal sensors for application of this approach to derive quantitative [Chl *a*]. Although the MERIS time-series ended in 2012, it provides ten years of ocean colour data for time-series analysis and algorithm development and testing. OLCI was built on MERIS heritage with similar radiometric setup and quality to ensure algorithm and data time-series continuity between these sensors.

The focus of this paper is to optimally resolve [Chl *a*] over a wide range of biomass in waters where phytoplankton are the dominant optical constituent in the water column (i.e. where the contributions from absorption and backscattering of terrigenous coloured dissolved organic particles and inorganic particles to the water-leaving signal are relatively small). The goal was not to derive new algorithms, but to find the best performing existing algorithms for low to moderate ( $< 10 \text{ mg m}^{-3}$ ), and moderate to high ( $> 10 \text{ mg m}^{-3}$ ) biomass waters, and to devise a method to assign, and where necessary blend, algorithm returns.

## 2. Materials and methods

### 2.1. *In situ* data collection

All the *in situ* data were collected in the southern Benguela along the west coast of South Africa between 2002 and 2017. This region has been the focus of many ocean colour remote sensing studies since 2002 due to the high productivity of the upwelling system and resulting harmful algal blooms. Field campaigns have most often focussed on the upwelling or highly productive seasons (February to April) in order to capture *in situ* and satellite validation data for the phytoplankton blooms which frequently occur during this time. The available data were collected during collaborative research efforts between the Department of Agriculture, Forestry and Fisheries (DAFF), the Council for Scientific and Industrial Research (CSIR) and the University of Cape Town (UCT) and have included data collection in the St Helena Bay region near Lambert's Bay ( $N = 142$ ), Elands Bay ( $N = 25$ ), and the Berg River mouth ( $N = 5$ ), as well as in Saldanha Bay ( $N = 6$ ). The methodological details for these field studies are all similar, and are described below. Additional data collected in the Benguela region includes the Benguela Calibration (BENCAL) cruise ( $N = 20$ ) during October 2002; details of the data collection methodology can be found in the cruise report (Barlow et al., 2003). A complete *in situ* dataset which focused on the  $R_{rs}$  and [Chl *a*] data was compiled from the aforementioned studies.

Coincident radiometric measurements and water sample collection were performed within maximum of 60 min (although usually within 30 min) of satellite overpass times, usually between 09:30 and 10:30 local time. In-water radiometric measurements were made with a hyperspectral Tethered Atlantic Radiometric Buoy (TSRB). The TSRB measures upwelling radiance ( $L_u(z)$  at  $z = -0.66 \text{ m } \mu\text{W cm}^{-2} \text{ nm}^{-1} \text{ sr}^{-1}$ ) and above surface downwelling irradiance ( $E_d(0^+)$ ,  $\mu\text{W cm}^{-2} \text{ nm}^{-1}$ ) and has two 256 channel spectrographs that cover a spectral range of 400 to 800 nm. During acquisition the instrument was floated far enough from the vessel to avoid shadowing or interference. Measurements were typically recorded for about 2 to 5 min. Raw data were processed with Prosoft 6.3d (Satlantic: Halifax, Canada); the median values of the deployment were selected and resampled to a spectral resolution of 5 nm. The measured radiometric variables were converted to remote sensing reflectance ( $R_{rs}$ ) using the equivalent algal population (EAP) inversion algorithm with Ecolight-S (Mobley, 2011) (as described in Evers-King et al., 2014) to derive the upwelling radiance attenuation coefficient ( $K_{Lu}$ ). Various sources of uncertainty can affect the derivation of *in situ*  $R_{rs}$ , including the cumulative uncertainty in upwelling radiance (Antoine et al., 2006), calibration uncertainty for irradiance (Zibordi and Voss, 2010), the self-shading percentage error of the TSRB (Leathers et al., 2001), and the tilt and roll of the instrument (Zibordi et al., 2012), to name a few. The cumulative uncertainty budget for these types of radiometric buoys has been

shown to vary between approximately 6.4 and 7.9% (Antoine et al., 2008; Smith et al., 2013; Zibordi et al., 2012) with the highest uncertainty in the red spectral region.

Chlorophyll *a* (Chl *a*) concentration was measured by fluorometric analysis (Holm-Hansen et al., 1965) using 90% acetone with the use of a Turner Designs 10-AU Fluorometer according to accepted protocols (Knap et al., 1996; Mueller et al., 2003). The uncertainty associated with the fluorometric derivation of Chl *a* can be in the order of approximately 50% (Trees et al., 1985; Smith et al., 2013). Although High Pressure Liquid Chromatography (HPLC) is considered as the preferred protocol for the determination of total chlorophyll (Roesler et al., 2017), most of the data used in this study were from historical datasets which only included fluorometric Chl *a*. The presence of Chl *c* in a primarily diatom and dinoflagellate dominated system such as the southern Benguela, would most likely cause an overestimation of [Chl *a*] when using fluorometric methods versus HPLC (Marrari et al., 2006); however, this type of overestimation has the greatest effect at low biomass ( $< 1.5 \text{ mg m}^{-3}$ ).

## 2.2. Satellite data

Reduced resolution (approximately 1.2 km pixels) level 2 data from the third reprocessing of MERIS were obtained from the MERIS catalogue and inventory (MERCI) website. Data from OLCI on board Sentinel-3A were obtained from a ftp site (<ftp://oda.eumetsat.int>) for Sentinel 3 validation team members; these data were from OLCI processing baseline 2.23 with IPF version 06.11. The bright pixel atmospheric correction (Moore and Lavender, 2011) is usually universally applied in both MERIS and OLCI images of the shelf waters of southern Benguela, and was applied to all extracted pixels. It should be noted that the OLCI data are not yet a stable data record at the time of publication. For both sensors, the normalized water-leaving reflectances were converted to remote sensing reflectance  $R_{rs}$  by dividing spectra by  $\pi$  (Antoine and Morel, 2005). Satellite data were extracted for the pixel closest to the *in situ* sampling station position, as well as the eight surrounding pixels, and a mean of the nine pixels was used for further calculations. A map of the matchup locations is provided in Fig. 1. Level 2 quality flags applied to MERIS satellite data products included land, cloud, high\_glint, ice\_haze, and/or PCD\_1\_13 (the confidence flag for the reflectances), whilst the confidence flag for the algal pigment index 1 products (PCD\_15) was applied to the derived Chl *a* data from the blue-green algorithm. Flags applied to OLCI data included invalid, land, cloud, cloudambiguous, cloudmargin, acfail, glint, and kdm\_fail, whilst oc4me\_fail was also applied to the derived Chl *a* data from the blue-green algorithm. Generally the above-mentioned flags would mask data with severe negative reflectances; however, additional failsafe mechanisms were implemented during Chl *a* algorithm application to satellite data, which will be discussed further in Section 4.2.

## 2.3. Chlorophyll *a* algorithms

The performance of several empirical algorithms were assessed across a variety of *in situ* [Chl *a*] (see Appendix A). Although it is acknowledged that waveband adjustment and regional tuning can improve the performance of these algorithms (e.g. Sun et al., 2014), the focus of this study was on the use of MERIS/OLCI wavebands with existing algorithms.

Two different empirical algorithms are used in this study. The first is a two-band red-NIR algorithm developed by Gilerson et al. (2010) chosen for application over primarily moderate to high biomass waters; the algorithm, which we will refer to as G2B, is defined as:

$$Chla = \frac{\left( \left( a_w(708) \times \frac{R_{708}}{R_{665}} \right) - a_w(665) \right)}{a_{ph}^*(665)} \quad (1)$$

where  $a_w$  is the water absorption at 708 ( $= 0.79 \text{ m}^{-1}$ ) and 665 nm

( $= 0.42 \text{ m}^{-1}$ ) respectively, and  $a_{ph}^*(665)$  is the phytoplankton specific absorption at 665 nm based on the following relationship (Gilerson et al., 2010):

$$a_{ph}^*(665) = (0.022[Chla])^{-0.1675}. \quad (2)$$

When presented in terms of Eqs. (1) and (2), the G2B algorithm is defined as:

$$Chla = \left( \left( 35.75 \times \frac{R_{708}}{R_{665}} \right) - 19.3 \right)^{1.124}. \quad (3)$$

The OCI algorithm (Hu et al., 2012), which is a combination of the Chlorophyll Index (CI) (Hu et al., 2012) and the OC4 (O'Reilly et al., 2000) algorithms, was selected for application over low to moderate biomass waters. The OCI utilizes the CI algorithm for  $Chl_{CI} < 0.25$ , OC4 for  $Chl_{CI} \geq 0.3$ , and a weighted blend of the two algorithms in between these values. For application to MERIS and OLCI, the CI algorithm is defined as:

$$CI = R_{rs}(560) - [R_{rs}(443) + (560 - 443)(665 - 443) * (R_{rs}(665) - R_{rs}(443))] \quad (4)$$

where CI can be converted to [Chl *a*] as follows:

$$Chl_{CI} (\text{mg m}^{-3}) = 10^{(-0.4909 + 191.6590 * CI)}. \quad (5)$$

The OC4 algorithm (or in this case the OC4E algorithm for MERIS) is defined as:

$$[Chl \ a] (\text{mg m}^{-3}) = 10^{(0.3255 - 2.7677 * X + 2.4409 * X^2 - 1.1288 * X^3 - 0.4990 * X^4)}. \quad (6)$$

where  $X$  is the log10 of the maximum ratio of the  $R_{rs}$  between either 443, 490, or 510, and 560 nm. The coefficients of the polynomial were derived for MERIS wavelengths from version 2 of the NASA bio-Optical Marine Algorithm Dataset (NOMAD) (Werdell and Bailey, 2005), and were obtained from Feldman and McClain (2017).

## 2.4. Statistical methods

Hyperspectral *in situ* and synthetic  $R_{rs}$  were interpolated to the appropriate MERIS and OLCI wavelengths of 443, 490, 510, 560, 665 and 708 nm. Chl *a* algorithms were applied to synthetic, *in situ* and satellite  $R_{rs}$ , and the resultant modeled [Chl *a*] were compared to the available known *in situ* and synthetic [Chl *a*] (the methods for the synthetic dataset will be described further in Section 2.5). The statistical descriptors used to assess individual and blended algorithm performance included the bias (the average difference), median absolute relative difference (MARD) and the root-mean-square difference (RMSD).

The bias is defined as:

$$\text{bias} = \frac{1}{N} \sum_{i=1}^N (\log_{10} Chl_{mod} - \log_{10} Chl_{insitu}) \quad (7)$$

the median absolute relative difference (MARD) is expressed in percentage as:

$$\text{MARD} = 100 * \text{median} \left[ \frac{|Chl_{mod} - Chl_{insitu}|}{Chl_{insitu}} \right] \quad (8)$$

and the root-mean-square difference (RMSD) as:

$$\text{RMSD} = \sqrt{\frac{1}{N} \sum_{i=1}^N (\log_{10} Chl_{mod} - \log_{10} Chl_{insitu})^2} \quad (9)$$

where  $Chl_{mod}$  is the algorithm-derived [Chl *a*] output and  $Chl_{insitu}$  is the *in situ* [Chl *a*]. Since the natural distribution of [Chl *a*] in the ocean is considered to be log-normal (Campbell, 1995), the calculation of the bias and RMSD were performed on log-transformed data.

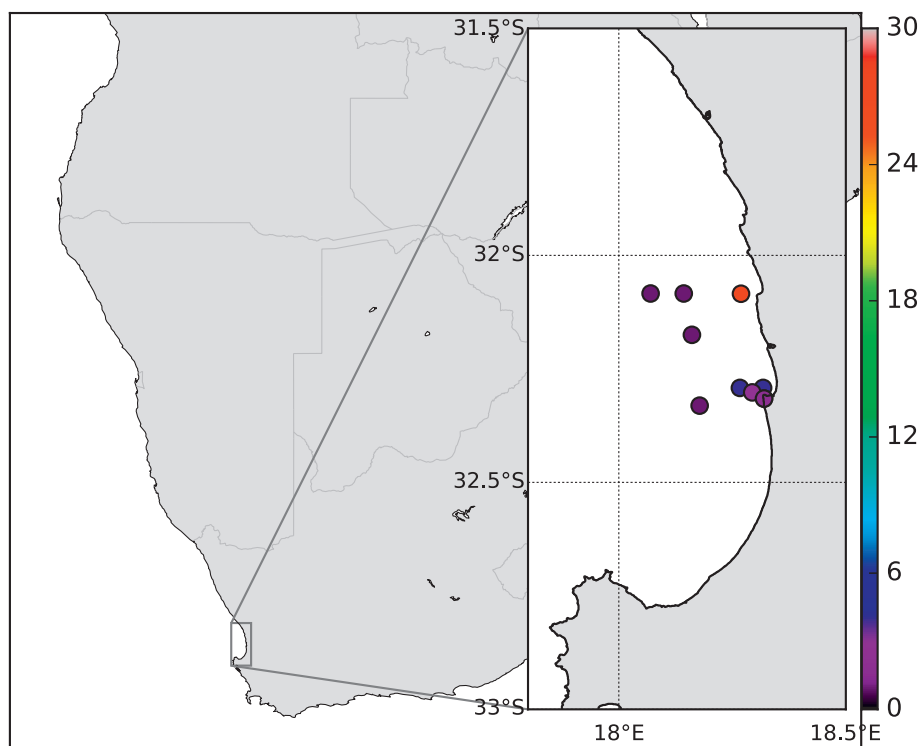


Fig. 1. Map of the *in situ* sampling locations with satellite match-ups in St Helena Bay, South Africa. The colour bar indicates the number of match-ups per sampling location. (For interpretation of the references to colour in this figure legend, the reader is referred to the web version of this article.)

## 2.5. Algorithm application and blending methods

Although red-NIR-centric algorithms are often preferred over blue-green algorithms in high biomass waters, these algorithms also have some limitations. At  $[\text{Chl } a] < 10 \text{ mg m}^{-3}$  the  $R_{rs}$  signal in the NIR can be small, resulting in a lower signal to noise ratio and larger measurement uncertainties (Dall'Olmo and Gitelson, 2006). Studies have also found that the generalized relationship between  $a_p^*$  and  $[\text{Chl } a]$ , upon which the G2B algorithm is based, changed rapidly at  $[\text{Chl } a]$  below approximately  $10 \text{ mg m}^{-3}$  (Gilerson et al., 2010; Shi et al., 2013). Previous studies have recommended a minimum threshold around  $10 \text{ mg m}^{-3}$   $[\text{Chl } a]$  for these types of 2 or 3 band red-NIR algorithms (Dall'Olmo and Gitelson, 2006; Moses et al., 2009a,b; Odermatt et al., 2012), which corresponds to a red-NIR ratio value of approximately 0.75 in the case of the G2B algorithm. Several studies (e.g. Matsushita et al., 2015; Gurlin et al., 2011) have also noted  $25 \text{ mg m}^{-3}$  as a theoretical boundary for these types of algorithms, whilst it is also typically considered to be the threshold between eutrophic and hypertrophic waters (Vollenweider and Kerekes, 1982).

A synthetic dataset was produced in order to assess the potential variability introduced by the application of the OCI algorithm and the red-NIR ratio to reflectance spectra representing phytoplankton of different effective cell diameters ( $D_{\text{eff}}$ ); the dataset consisted of 500 reflectance spectra at 5 nm intervals. These spectra were created with IOPs from the Equivalent Algal Populations phytoplankton model as described in Robertson Lain et al. (2014) and modeled to  $R_{rs}$  using EcoLight radiative transfer code (Mobley and Sundman, 2008). 100 spectra of  $\text{Chl } a$  concentration steps between 1 and  $100 \text{ mg m}^{-3}$  were produced to simulate generalized eukaryotic assemblages (Robertson Lain et al., 2014) with  $D_{\text{eff}}$  of 6, 12, 18, 24, and  $32 \mu\text{m}$ ; these effective diameters are generally representative of assemblage types that might be found in the southern Benguela, although each  $D_{\text{eff}}$  may not naturally occur at all the  $[\text{Chl } a]$  presented in Fig. 2. The large dispersal of the curves represent both the effects of  $D_{\text{eff}}$  and the use of the OCI algorithm. As these data do not represent the appropriate allometric scaling

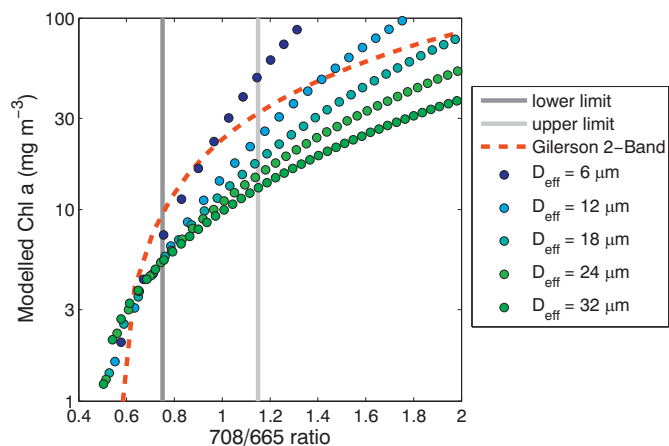


Fig. 2. Plot showing the relationship between the 708/665 nm ratio and modeled  $[\text{Chl } a]$  from the OCI algorithm for the synthetic  $R_{rs}$  spectra of cells with effective diameters of 6, 12, 18, 24, and  $32 \mu\text{m}$ . The red dashed line represents the G2B red-NIR algorithm, whilst the dark and light grey lines show the lower and upper limit of the ratio, respectively, between which the weighted blend occurs. (For interpretation of the references to colour in this figure legend, the reader is referred to the web version of this article.)

that is generally found in natural waters (Agusti et al., 1987), the synthetic dataset is used for illustrative purposes and not for specific algorithm testing in this study. CDOM and non-algal (back)scattering was modeled following (Robertson Lain et al., 2014). The phytoplankton specific absorption ( $a_{ph}^*$ ) at 675 nm for the synthetic dataset ranged between 0.0117 and  $0.0231 \text{ m}^2 \text{ mgChl}^{-1}$  for  $D_{\text{eff}}$  of 32 and  $6 \mu\text{m}$  respectively, which falls within the bounds of the data used to derive and assess the G2B algorithm (Gilerson et al., 2010).

The range of algorithm blending was assessed by varying the lower limits between 0.6 and 0.9 and upper limits between 0.8 and 1.2 during the application of the blending procedure (using G2B and OCI); this was



**Table 1**The statistical descriptors of the *in situ* 709/665 nm ratio for three different groups of [Chl *a*].

Biomass group	Min	25th percentile	Median	Mean	75th percentile	Max	Stdev	N
Chl <i>a</i> ≤ 10 mg m <sup>-3</sup>	0.49	0.53	0.58	0.61	0.66	1.03	0.10	96
10 < Chl <i>a</i> ≤ 25 mg m <sup>-3</sup>	0.56	0.75	0.92	0.98	1.15	2.30	0.32	41
Chl <i>a</i> > 25 mg m <sup>-3</sup>	0.79	1.09	1.39	2.15	3.12	5.43	1.46	26

done for both *in situ* and satellite matchup datasets. Within these limits the *in situ* and satellite data showed RMSD of 0.263–0.275 and 0.343–0.366 respectively, and MARD of 34.4–39.1 % and 41.7–45.7 % respectively. The variations in algorithm blending performance were relatively small in comparison to the performance of the single algorithms. Furthermore, the *in situ* dataset was divided into three different groups of [Chl *a*] ≤ 10 mg m<sup>-3</sup>, 10 < [Chl *a*] ≤ 25 mg m<sup>-3</sup>, and [Chl *a*] > 25 mg m<sup>-3</sup>, as done in Matsushita et al. (2015), in order to assess the statistical descriptors of the 708/665 nm ratio under different phytoplankton biomass levels; these results are shown in Table 1.

The choice of 0.75 and 1.15 represented the 25th and 75th percentiles of the *in situ* data that fell into the 10 < [Chl *a*] ≤ 25 mg m<sup>-3</sup> group. This blending range showed good visual synoptic coherency when applied to satellite data of a variety of known bloom events in the southern Benguela. As seen in Fig. 2 the lower limit for the G2B algorithm and blending procedure corresponds to approximately 10 mg m<sup>-3</sup>, whilst the upper limit for the OCI algorithm theoretically still falls within the operational limits of the blue-green algorithms (i.e. < 25 mg m<sup>-3</sup>) even for smaller cells. In between ratio values of 0.75 and 1.15 the two algorithms are blended using a weighted approach:

$$Chl_{blend}(mg\ m^{-3}) = \alpha_1 * Chl_{G2B} + \alpha_2 * Chl_{OCI} \quad (10)$$

where  $\alpha_1 = (\phi - 0.75)/(1.15 - 0.75)$ ;  $\alpha_2 = (1.15 - \phi)/(1.15 - 0.75)$ ; and  $\phi = R_{rs}(708)/R_{rs}(665)$ .

### 3. Results

The statistical results of the comparison of algorithm performance for both *in situ* and satellite  $R_{rs}$  data collected in the southern Benguela, are given in Table 2. For *in situ* data the blended product shows the lowest RMSD and MARD, with a slightly positive bias. The G2B shows a lower RMSD than OCI for both the *in situ* and the satellite data. When applied to *in situ* data, the blend also shows better MARD results for the southern Benguela (36.4%, from Table 2) compared to the regionally-tuned EAP algorithm, which had an absolute percentage error of 73% (Evers-King, 2014) relative to *in situ* [Chl *a*]. For the satellite data the G2B shows slightly lower RMSD and MARD than the blended product; however, there are a number of datapoints lost when applying the G2B algorithm (32 and 9 datapoints in the *in situ* and satellite datasets respectively) due to noisy or low red-NIR signal resulting in negative [Chl *a*] returns at low biomass.

The characteristics of the Chl *a* for the *in situ* and matchup data are

**Table 2**

The root mean squared difference (RMSD), median absolute relative difference (MARD), bias, and number of positive modeled results (*N*) used for comparing returned Chl *a* (from algorithms applied to *in situ* and satellite  $R_{rs}$  respectively) to *in situ* Chl *a*. RMSD and bias are given in log10 units.

Source	Chl <i>a</i> algorithm	RMSD	MARD [%]	Bias	N
<i>In situ</i> $R_{rs}$	OCI	0.448	39.8	0.022	163
	G2B	0.386	44.5	-0.060	131
	Blend	0.268	37.9	0.020	163
Satellite $R_{rs}$	OCI	0.388	49.9	-0.064	51
	G2B	0.336	35.6	-0.067	42
	Blend	0.351	45.7	-0.014	51

**Table 3**

The characteristics of the *in situ* Chl *a* data, as well as the *in situ* data with satellite matchups (provided in mg m<sup>-3</sup>). Please note that any data points with satellite matchups were removed from the *in situ* dataset.

Dataset	Minimum	Median	Mean	Maximum	Stdev	N
<i>Chl<sub>in situ</sub></i>	0.25	6.8	18.3	201.6	34.5	163
<i>Chl<sub>matchup</sub></i>	0.43	11.7	25.7	309.0	53.7	51

provided in Table 3. Although both datasets show similar ranges, the satellite data generally represented slightly higher biomass; the relatively high mean values in both datasets may explain why the red-NIR algorithm generally shows better performance than the OCI. Due to its increased functional range and ability to utilize most of the available data, the blend would be the preferred product in the southern Benguela.

Scatterplots demonstrating the blending and weighting procedure for both datasets are provided in Fig. 3. Most of the scatter around the 1:1 line, particularly in the satellite matchup dataset, appears to occur within the operational bounds of the individual algorithms, whilst the blended returns are more closely related to *in situ* values.

## 4. Discussion

### 4.1. Chlorophyll algorithm suitability

Blue-green empirical algorithms have frequently been utilized in the southern Benguela (Machu et al., 1999; Demarcq et al., 2003; Weeks et al., 2006; Silió-Calzada et al., 2008), although only sporadically validated in this region (e.g. Aiken et al., 2007). Due to the frequent moderate to high biomass found in the shelf waters, algorithms operating in the red-NIR (Bernard et al., 2005; Matthews et al., 2012) or regionally parameterized inversion algorithms (Evers-King, 2014) offer better operational ability to capture the full extent of high biomass blooms. Although the three-band red-NIR algorithm (Gilerson et al., 2010) (which uses 665, 708 and 753 nm) was also considered for use in the region, studies have shown that the two-band algorithm produces improved results (Gurlin et al., 2011), particularly over lower biomass waters where the use of the 753 nm band may increase the impact of low sensor signal-to-noise ratio and atmospheric correction problems on algorithm performance (Yacobi et al., 2011).

Red-NIR algorithms may not operate optimally in low biomass waters, represented by freshly upwelled or offshore conditions in the southern Benguela; although accurate [Chl *a*] retrieval < 10 mg m<sup>-3</sup> has been demonstrated for 708/665 nm algorithms (Gurlin et al., 2011), in practice the operational application to satellite data can often produce negative or unrealistic returns when the reflectance signal from phytoplankton approaches the sensor noise level in the red-NIR. International projects have integrated blue-green empirical algorithms for use over these water types; the OC4E algorithm is used for clear and moderately turbid waters in MERIS data from the Coast Colour project (Brockmann, 2014), whilst the OCI algorithm forms part of the OC-CCI Chl *a* algorithm blending procedure (Grant et al., 2015). Although the MERIS algal1 product and the OLCI CHL\_OC4ME product (Morel and Antoine, 2011) also use a similar algorithm format, the OC4E algorithm (as used within OCI) produced lower RMSD, MARD and bias values when applied to the *in situ* data (see Appendix A); this is potentially due

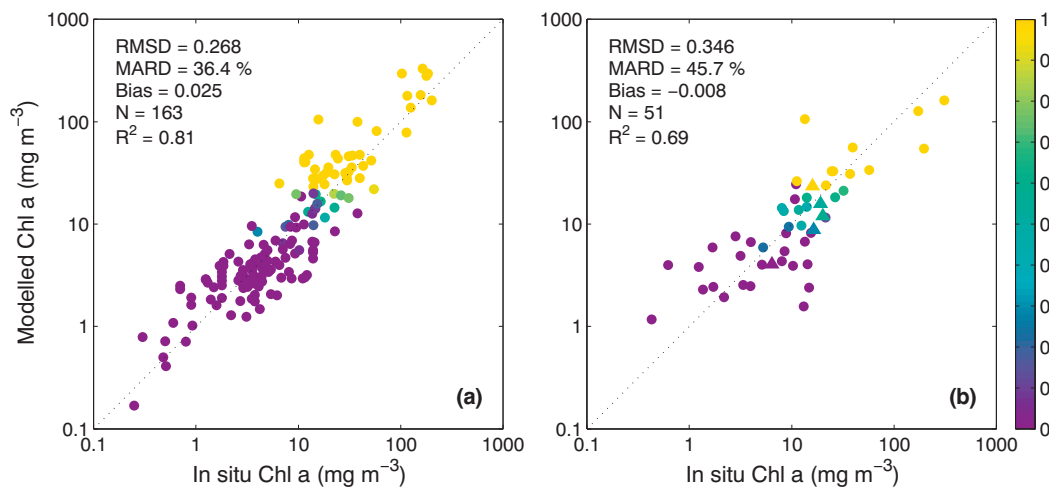


**Fig. 3.** Scatterplot showing the relationship between *in situ* Chl *a* and the modeled Chl *a* obtained by application of the switching and blending method to (a) *in situ* and (b) satellite-derived reflectance from MERIS ( $N = 46$ , circles) and OLCI ( $N = 5$ , triangles). The colour bar indicates the weighting of the G2B algorithm (i.e. a weighting of zero means that only OCI was applied). (For interpretation of the references to colour in this figure legend, the reader is referred to the web version of this article.)

to the large range ( $0.012$  to  $72.1 \text{ mg m}^{-3}$ ) and increased number of data points with  $[\text{Chl } a] > 20 \text{ mg m}^{-3}$  in the NOMAD v2 dataset (Werdell and Bailey, 2005), making the derived coefficients used for OC4E potentially more suitable for use in the southern Benguela than standard MERIS and OLCI Case 1 products.

The OC4E and G2B algorithms have previously been included in a hybrid switching algorithm for Asian Lakes (Matsushita et al., 2015), where the switch is based on the maximum chlorophyll index (MCI, Gower et al., 2005), whilst OC4E and G2B are utilized for  $[\text{Chl } a]$  ranges of  $< 10 \text{ mg m}^{-3}$  and  $10\text{--}25 \text{ mg m}^{-3}$  respectively.

#### 4.2. Switch and blending suitability

A number of other methods were considered to trigger the algorithm switch. The first option was an OC4-based switch (i.e. using  $[\text{Chl } a]$  values of approximately  $10$  and  $25 \text{ mg m}^{-3}$  as lower and upper limits respectively). However, this method was abandoned, as basing a switch on a derived product could potentially compound uncertainties (i.e. those from atmospheric correction and algorithm application). Furthermore, many satellite pixels representing high biomass waters are often flagged in the OCI product due to algorithm failure, which would disrupt the blending procedure and potentially produce hard boundaries in the imagery.

Other options included switching on the MCI value as done in Matsushita et al. (2015), or on the three-band red-NIR ratio (Gilerson et al., 2010). However, a reflectance ratio-based approach between wavebands in close proximity to each other provides more accurate results at low  $[\text{Chl } a]$ , as there is a smaller impact from the potential effects of spectral non-uniformity of the backscattering coefficient (Yacobi et al., 2011). Since the lower limit of the ratio-based switch ( $0.75$ ) is set above the theoretical lower limit for the G2B algorithm (approximately  $0.6$ ), a smooth transition should always be possible with valid satellite  $R_{rs}$  spectra. Additional failsafe mechanisms for application to satellite data include the use of only reflectance spectra with  $R_{rs}(665) > 0 \text{ sr}^{-1}$ , as well as discarding pixel values where the ratio is  $> 1.2$  whilst  $R_{rs}(665)$  is  $> 0.0005 \text{ sr}^{-1}$ ; this was done in an attempt to discard invalid spectra that may not have been caught by the applied data quality flags, and was performed for satellite matchups as well as subsequent algorithm application to satellite images. Corrected sun glint appeared to affect the reliability of the ratio; as a result only the blue-green algorithm is used when the medium glint flag is raised.

As demonstrated in Table 2 the use of the two different algorithms together with the blending procedure produces improved results, either

by providing lower uncertainty  $[\text{Chl } a]$  returns or through increased data (or satellite pixel) availability.

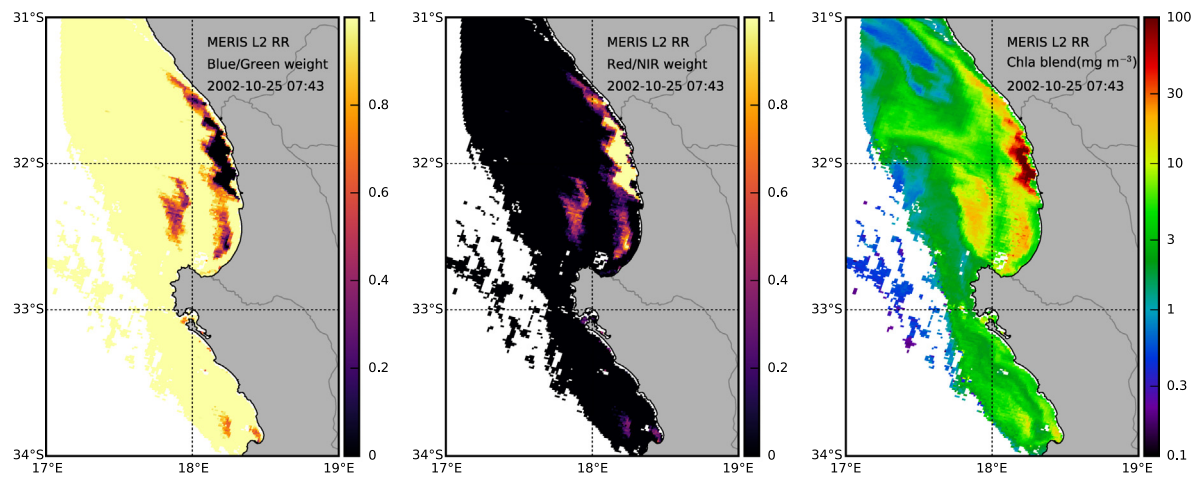
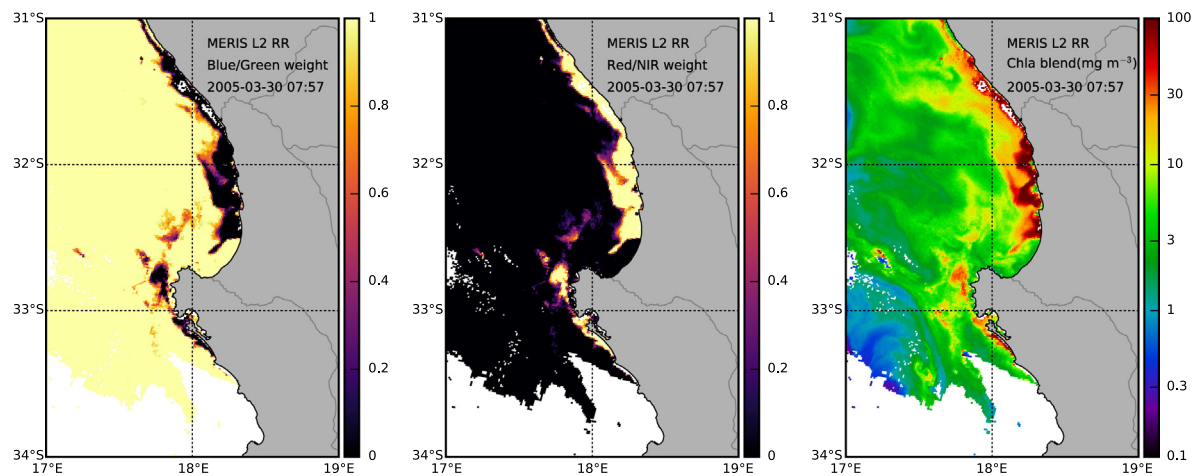
#### 4.3. Blending algorithm application examples

Fig. 4 demonstrates the algorithm weighting and blending for three high biomass dinoflagellate bloom events that have been captured by MERIS (panels a and b) and OLCI (c) in St Helena Bay. Panel (a) shows an *Alexandrium catenella* bloom, whilst panel (b) represents mixed assemblages including toxic species such as *Dinophysis* spp. and *Prorocentrum reticulatum*, as well as non-toxic species *Prorocentrum triestinum* (Fawcett et al., 2007). *In situ* samples taken during both these events measured  $[\text{Chl } a] > 100 \text{ mg m}^{-3}$  (Fawcett et al., 2007; Bernard et al., 2014). Panel (c) shows a high biomass bloom of *Ceratium* sp. (personal communication, Dr. Grant Pitcher). Although no *in situ* measurements were taken on the day,  $[\text{Chl } a]$  values were  $> 50 \text{ mg m}^{-3}$  in the south of the Bay on the 11th of May, whilst this bloom remained in the vicinity until early June. In all three examples the spatial extent and intensity of the blooms, as well as the lower biomass offshore waters, are well represented by the blended product.

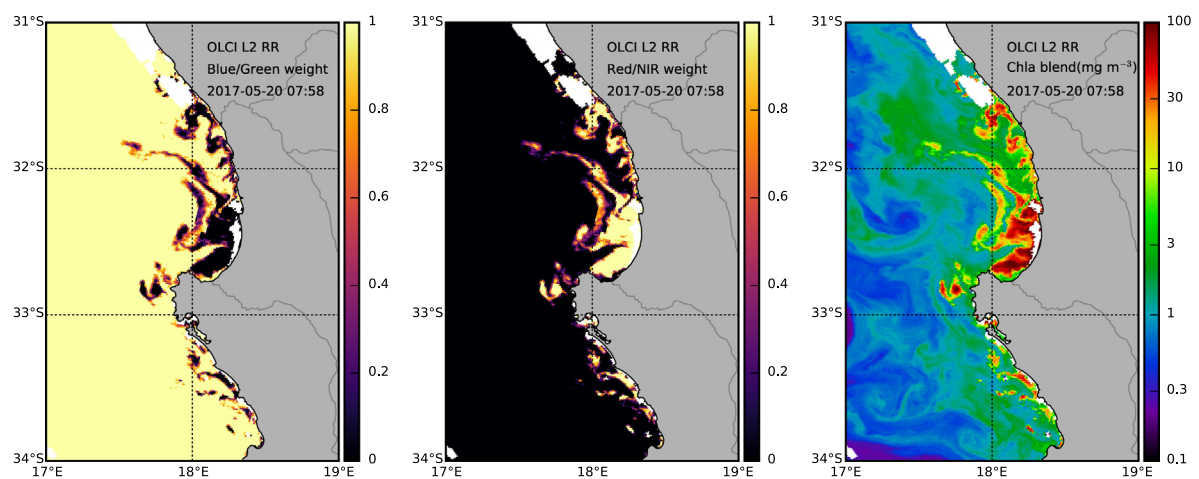
The majority of each image is resolved with the blue-green algorithm, whilst only the high biomass bloom areas near the coast necessitate the use of the red-NIR algorithm. Histograms of each image in Fig. 4 are provided in Fig. 5; these plots demonstrate both the larger number of valid  $[\text{Chl } a]$  returns and the increased operational range of the blended product compared to the individual algorithms. Both Figs. 4 and 5 show a smooth transition between the two algorithms, demonstrating the efficacy of the ratio-based blending technique. The blended products will be incorporated into operational processing chains for HAB detection along the west and south coasts of South Africa.

#### 4.4. Algorithm and blending limitations

Although the G2B is not very sensitive to the influence from  $a_{cdom}$  and  $b_b$  (Gilerson et al., 2010), this is not the case with most standard blue-green empirical algorithms; application of the specific ratio-based blending technique outlined in this study in waters where phytoplankton is not the dominant optical variable would likely necessitate the replacement of OCI with a suitable alternative — possibly a regionally or water type specific parameterized semianalytical algorithm (e.g. Moore et al., 2001; Le et al., 2011) or neural network (e.g. Vilas et al., 2011; Brockmann, 2014).

(a) Envisat MERIS RR - *Alexandrium catanella*

(b) Envisat MERIS - Mixed dinoflagellate

(c) Sentinel3A OLCI - *Ceratium sp.*

**Fig. 4.** Examples of algorithm blending application for reduced resolution MERIS reflectance on the 25th of October 2002 (a) and the 30th of March 2005 (b), as well as for OLCI on the 10th of May 2017 (c). Panels on the left and centre show the weighting used to blend the OCI and G2B algorithms respectively, with the final blended Chl *a* product on the right.

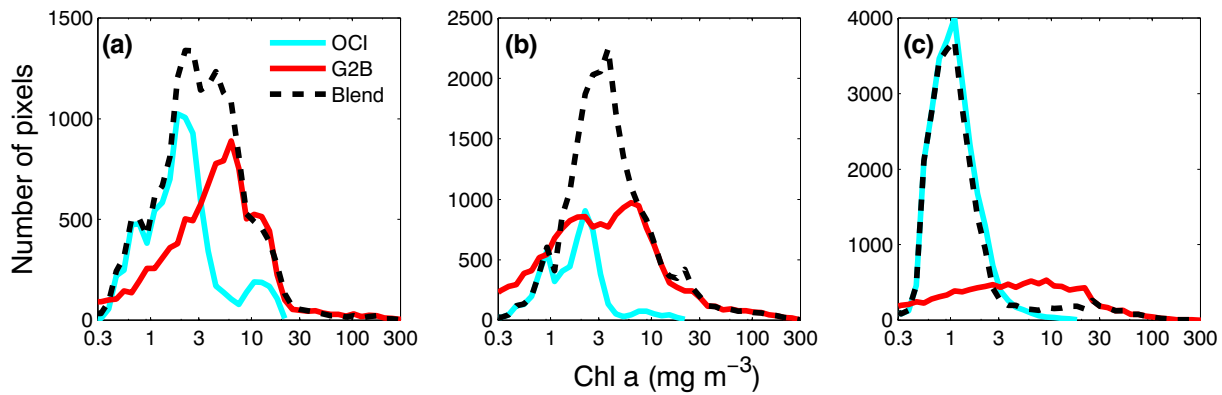


Fig. 5. Histograms of the [Chl *a*] returns from the OC4E, Gilerson 2-band (G2B) and the ratio-based blend of the two algorithms, corresponding to the panel numbers in Fig. 4.

It is foreseeable that the algorithm blending technique with the same algorithms could be applied as is to other phytoplankton dominated waters, e.g. California and some inland water bodies. It is possible that the upper and lower limits of the algorithms need to be adjusted according to local optical water types in order to produce regionally-optimized results.

As with all reflectance-based algorithms, the successful application of the switch and the individual algorithms are dependent on the accuracy of the applied atmospheric correction. After the recent OLCI reprocessing average relative percent differences of below 5% have been recorded for reflectance bands between 443 and 560 nm, and between 3 and 7% for 665 nm (EUMETSAT, 2018). However, problems have been reported with the bright pixel correction (BPAC) when applied to OLCI data, which can result in erroneous reflectances (EUMETSAT, 2018). Since BPAC is generally applied over the southern Benguela, other atmospheric correction methods may need to be considered in future. One such option is POLYMER (Steinmetz et al., 2011) which has been used with MERIS and has shown promising results in the red, NIR, and for the 709/665 nm reflectance ratio in highly absorbing waters (Qin et al., 2017).

## Appendix A

Several known Chl *a* algorithms were considered for use in this study. They were tested by statistical comparison of the known *in situ* [Chl *a*], to the [Chl *a*] returned by algorithm application to *in situ*  $R_{rs}$ . Brief descriptions and references for all the algorithms are provided in Table A.4.

Table A.4

Descriptions of the algorithms used in this study. The coefficients for the OC3E, OC4E, and OC5E algorithms were derived for MERIS wavelengths from version 2 of the NASA bio-Optical Marine Algorithm Dataset (NOMAD) (Werdell and Bailey, 2005), and were obtained from Feldman and McClain (2017).

Algorithm	Description
OC3E (O'Reilly et al., 2000)	A three-band blue-green reflectance ratio of the following format: $X = \log_{10}([R_{rs}(443) > R_{rs}(490)]/R_{rs}(560))$ $Chla = 10^{(a_0 + a_1X + a_2X^2 + a_3X^3 + a_4X^4)}$ with coefficients: $a_0 = 0.2521$ , $a_1 = -2.2146$ , $a_2 = 1.5193$ , $a_3 = -0.7702$ , $a_4 = -0.4291$
OC4E (O'Reilly et al., 2000)	A four-band blue-green reflectance ratio of the following format: $X = \log_{10}([R_{rs}(443) > R_{rs}(490) > R_{rs}(510)]/R_{rs}(560))$ $Chla$ is determined in the same way as OC3E using the following coefficients: $a_0 = 0.3255$ , $a_1 = -2.7677$ , $a_2 = 2.4409$ , $a_3 = -1.1288$ , $a_4 = -0.4990$
OC4Me (Morel and Antoine, 2011)	The algorithm is similar to OC4E, using the following coefficients: $a_0 = 0.4502748$ , $a_1 = -3.259491$ , $a_2 = 3.522731$ , $a_3 = -3.359422$ , $a_4 = 0.949586$
OC5E (Gohin et al., 2002)	$Chla$ is determined by means of a triplet of the OC4E, $nLw(412)$ , $nLw(560)$ based on a look-up table
Gu2B (Gurlin et al., 2011)	$2BandModel = R_{665}^{-1} \times R_{709}$ $Chla = 25.28 \times (2BandModel)^2 + 14.85 \times (2BandModel) - 15.18$

(continued on next page)



Table A.4 (continued)

Algorithm	Description
G2B (Gilerson et al., 2010)	$2BandModel = R_{665}^{-1} \times R_{709}$ $Chla = ((35.75 \times 2BandModel) - 19.30)^{1.124}$
G3B (Gilerson et al., 2010)	$3BandModel = (R_{665}^{-1} - R_{709}^{-1}) \times R_{753}$ $Chla = ((113.36 \times 3BandModel) + 16.45)^{1.124}$
L4B (Le et al., 2013)	$4BandModel = [1/R_{rs}(708) - 1/R_{rs}(665)]/[1/R_{rs}(708) - 1/R_{rs}(665)]$ $Chla = (20.55 \times 4BandModel) + 5.23$
NDCI (Mishra and Mishra, 2012)	$NDCI = [R_{rs}(708) - R_{rs}(665)]/[R_{rs}(708) + R_{rs}(665)]$ $Chla = 14.039 + (86.115 \times NDCI) + (194.325 \times NDCI^2)$
SCI (Shen et al., 2010)	$H_{chl} = \left[ R_{rs}(\lambda_4) + \frac{\lambda_4 - \lambda_3}{\lambda_4 - \lambda_2} (R_{rs}(\lambda_2) - R_{rs}(\lambda_4)) \right] - R_{rs}(\lambda_3)$ $H_{\Delta} = R_{rs}(\lambda_2) - \left[ R_{rs}(\lambda_4) + \frac{\lambda_4 - \lambda_2}{\lambda_4 - \lambda_1} (R_{rs}(\lambda_1) - R_{rs}(\lambda_4)) \right]$ $SCI = H_{chl} - H_{\Delta}$ where $\lambda_1, \lambda_2, \lambda_3$ and $\lambda_4$ are 560, 620, 665, and 681 nm, respectively The following relationship between Chl <i>a</i> and SCI for MERIS wavelengths was obtained from Le et al. (2013): $Chla = 0.057 \times SCI^{-0.6327}$

Table A.5 provides the statistical results from the assessment of the Chl *a* algorithms listed in Table A.4. The algorithms were applied to the entire *in situ* reflectance dataset; however, in order to assess algorithm performance at different phytoplankton biomass levels, results are also provided for low biomass ( $[Chl\ a] \leq 10\ mg\ m^{-3}$ ), low to moderate ( $[Chl\ a] \leq 25\ mg\ m^{-3}$ ), moderate to high ( $[Chl\ a] > 10\ mg\ m^{-3}$ ), and high biomass ( $[Chl\ a] > 25\ mg\ m^{-3}$ ) conditions. The OC4E algorithm showed good performance (Table A.5) for the low and low to moderate biomass ranges, whereas the G2B performed better in the moderate to high and high biomass datasets respectively. The OC4E and G2B and were subsequently chosen for application in this study.

Table A.5

The root mean squared difference (RMSD), median absolute relative difference (MARD), bias, and number of positive modeled results (N) used for comparing returned Chl *a* (from algorithms applied to *in situ*  $R_{rs}$ ) to *in situ* Chl *a*. Results are shown for *in situ* data with  $[Chl\ a] \leq 10\ mg\ m^{-3}$ ,  $\leq 25\ mg\ m^{-3}$ ,  $> 10\ mg\ m^{-3}$ ,  $> 25\ mg\ m^{-3}$ , and for the entire dataset. RMSD and bias are given in log10 units.

Source	Chl <i>a</i> algorithm	RMSD	MARD [%]	Bias	N
<i>In situ</i> $[Chl\ a] \leq 10\ mg\ m^{-3}$	OC3E	0.242	31.2	−0.013	96
	OC4Me	0.307	53.7	0.178	96
	OC4E	0.227	29.2	0.014	96
	OC5E	0.269	41.4	0.134	96
	Gu2B	0.368	42.8	−0.073	65
	G2B	0.406	45.6	−0.145	64
	G3B	0.504	44.2	−0.215	24
	L4B	0.590	195.2	0.529	96
	NDCI	0.453	42.3	0.272	96
	SCI	0.378	44.3	0.046	96
<i>In situ</i> $[Chl\ a] \leq 25\ mg\ m^{-3}$	OC3E	0.323	33.8	−0.049	137
	OC4Me	0.425	63.0	0.203	137
	OC4E	0.295	34.0	−0.015	137
	OC5E	0.279	42.5	0.075	137
	Gu2B	0.394	48.9	−0.020	106
	G2B	0.417	49.3	−0.082	105
	G3B	0.526	65.8	−0.100	63
	L4B	0.509	158.0	0.426	137
	NDCI	0.419	47.5	0.159	137
	SCI	0.501	67.4	−0.177	137
<i>In situ</i> $[Chl\ a] > 10\ mg\ m^{-3}$	OC3E	0.668	63.3	−0.045	67
	OC4Me	1.306	100.6	0.587	67
	OC4E	0.643	54.2	0.034	67
	OC5E	0.530	47.4	0.000	67
	Gu2B	0.400	56.3	0.102	67
	G2B	0.366	40.1	0.020	67
	G3B	0.438	51.1	0.004	65
	L4B	0.205	52.3	0.046	67

(continued on next page)

Table A.5 (continued)

Source	Chl <i>a</i> algorithm	RMSD	MARD [%]	Bias	N
<i>In situ</i> [Chl <i>a</i> ] > 25 mg m <sup>-3</sup>	NDCI	0.307	45.3	−0.128	67
	SCI	0.978	84.7	−0.915	67
	OC3E	0.904	76.7	0.093	26
	OC4Me	1.948	182.8	1.102	26
	OC4E	0.894	72.8	0.217	26
	OC5E	0.761	68.8	0.100	26
	Gu2B	0.345	48.6	0.161	26
	G2B	0.215	30.1	0.027	26
	G3B	0.214	29.2	0.054	26
	L4B	0.326	65.9	−0.176	26
	NDCI	0.273	34.4	−0.165	26
	SCI	1.292	93.2	−1.254	26
<i>All in situ</i>	OC3E	0.467	44.6	−0.026	163
	OC4E	0.870	69.3	0.346	163
	OC4Me	0.448	39.8	0.022	163
	OC5E	0.398	44.4	0.079	163
	Gu2B	0.385	48.9	0.016	132
	G2B	0.386	44.5	−0.060	131
	G3B	0.457	49.6	−0.055	89
	L4B	0.376	139.6	0.330	163
	NDCI	0.400	43.5	0.107	163
	SCI	0.691	73.9	−0.349	163

## References

- Agusti, S., Duarte, C.M., Kalf, J., 1987. Algal cell size and the maximum density and biomass of phytoplankton. *Limnol. Oceanogr.* 32, 983–986.
- Aiken, J., Fishwick, J., Lavender, S., Barlow, R., Moore, G., Sessions, H., Bernard, S., Ras, J., Hardman-Mountford, N., 2007. Validation of MERIS reflectance and chlorophyll during the Bencal cruise October 2002: preliminary validation of new demonstration products for phytoplankton functional types and photosynthetic parameters. *Int. J. Remote Sens.* 28, 497–516.
- Antoine, D., Chami, M., Claustre, H., Ortenzio, F., Morel, A., Bécu, G., Gentili, B., Louis, F., Ras, J., Roussier, E., Scott, A.J., Tailliez, D., Hooker, S.B., Guevel, P., Desté, J.-F., Dempsey, C., Adams, D., 2006. BOUSSOLE: A Joint CNRS-INSU, ESA, CNES, and NASA Ocean Color Calibration and Validation Activity. Technical Report December. NASA.
- Antoine, D., d'Ortenzio, F., Hooker, S.B., Bécu, G., Gentili, B., Tailliez, D., Scott, A.J., 2008. Assessment of uncertainty in the ocean reflectance determined by three satellite ocean color sensors (MERIS, SeaWiFS and MODIS-A) at an offshore site in the Mediterranean Sea (Boussole Project). *J. Geophys. Res. Oceans* 113.
- Antoine, D., Morel, A., 2005. MERIS ATBD 2.7. Atmospheric correction of the MERIS observations over ocean Case 1 waters. Issue 5, Revision 0.
- Barlow, R., 1982. Phytoplankton ecology in the southern Benguela current. I. Biochemical composition. *J. Exp. Mar. Biol. Ecol.* 63, 209–227.
- Barlow, R., Sessions, H., Silulwane, N., Engel, H., Hooker, S., Aiken, J., Fishwick, J., Vicente, V., Morel, A., Chami, M., et al., 2003. BENCAL cruise report. SeaWiFS Postlaunch Tech. Rep. Ser. 27, 1–64.
- Bernard, S., Balt, C., Pitcher, G., et al., 2005. The use of MERIS for harmful algal bloom monitoring in the southern Benguela. In: MERIS (A) ATSR Workshop 2005. vol. 597. pp. 26.
- Bernard, S., Pitcher, G., Evers-King, H., Robertson, L., Matthews, M., Rabagliati, A., Balt, C., 2014. Ocean Colour Remote Sensing of Harmful Algal Blooms in the Benguela System. In: *Remote Sensing of the African Seas*. Springer, pp. 185–203.
- Brockmann, C., 2014. DUE CoastColour Product User Guide. Version 2 Revision 2. DUE CoastColour Product User Guide. Version 2 Revision 2.
- Campbell, J.W., 1995. The lognormal distribution as a model for bio-optical variability in the sea. *J. Geophys. Res. Oceans* (1978–2012) 100, 13237–13254.
- Carder, K.L., Chen, F., Lee, Z., Hawes, S., Kamykowski, D., 1999. Semianalytic moderate-resolution imaging spectrometer algorithms for chlorophyll *a* and absorption with bio-optical domains based on nitrate-depletion temperatures. *J. Geophys. Res. Oceans* 104, 5403–5421.
- D'Alimonte, D., Mélin, F., Zibordi, G., Berthon, J.-F., 2003. Use of the novelty detection technique to identify the range of applicability of empirical ocean color algorithms. *IEEE Trans. Geosci. Remote Sens.* 41, 2833–2843.
- Dall'Olmo, G., Gitelson, A.A., 2006. Effect of bio-optical parameter variability and uncertainties in reflectance measurements on the remote estimation of chlorophyll-*a* concentration in turbid productive waters: modeling results. *Appl. Opt.* 45, 3577–3592.
- Demarcq, H., Barlow, R.G., Shillington, F. a., 2003. Climatology and variability of sea surface temperature and surface chlorophyll in the Benguela and Agulhas ecosystems as observed by satellite imagery. *Afr. J. Mar. Sci.* 25, 363–372. <http://dx.doi.org/10.2989/18142320309504022>.
- Dierssen, H.M., 2010. Perspectives on empirical approaches for ocean color remote sensing of chlorophyll in a changing climate. *Proc. Natl. Acad. Sci. U. S. A.* 107, 17073–17078. <http://www.pubmedcentral.nih.gov/articlerender.fcgi?artid=2951429&tool=pmcentrez&rendertype=abstract><http://dx.doi.org/10.1073/pnas.0913800107>.
- EUMETSAT, 2018. Sentinel-3A Product Notice — OLCI Level-2 Ocean Colour Operational Products and Full-mission Reprocessed Time Series. Product notice ID EUM/OPS-SEN3/DOC/17/964713, Version 1.0. Sentinel-3A Product Notice — OLCI Level-2 Ocean Colour Operational Products and Full-mission Reprocessed Time Series. Product notice ID EUM/OPS-SEN3/DOC/17/964713, Version 1.0.
- Evers-King, H., 2014. Phytoplankton Community Structure Determined Through Remote Sensing and In Situ Optical Measurements. Ph.D. thesis. University of Cape Town.
- Evers-King, H., Bernard, S., Lain, L.R., Probyn, T.A., 2014. Sensitivity in reflectance attributed to phytoplankton cell size: forward and inverse modelling approaches. *Opt. Express* 22, 11536–11551.
- Fawcett, R., Pitcher, G., Bernard, S., Cembella, A., Kudela, R., et al., 2007. Contrasting wind patterns and toxigenic phytoplankton in the southern Benguela upwelling system. *Mar. Ecol. Prog. Ser.* 348, 19–31.
- Feldman, G., McClain, C., 2017. *Chlorophyll a (chlora)*. [https://oceancolor.gsfc.nasa.gov/atbd/chlor\\_a/](https://oceancolor.gsfc.nasa.gov/atbd/chlor_a/) [2017-06-30]. Accessed: 2017-07-03.
- Gitelson, A. a., Gitelson, A. a., Zhou, J., Gurlin, D., Moses, W., Ioannou, I., Ahmed, S. a., 2010. Algorithms for remote estimation of chlorophyll-*a* in coastal and inland waters using red and near infrared bands. *Opt. Express* 18, 24109–24125. <http://dx.doi.org/10.1364/OE.18.024109>.
- Gitelson, A.A., Gurlin, D., Moses, W., Yacobi, Y., 2011. Remote estimation of chlorophyll-*a* concentration in inland, estuarine, and coastal waters. In: *Advances in Environmental Remote Sensing: Sensors, Algorithms, and Applications*. CRC Press Taylor and Francis Group.
- Gohin, F., Druon, J., Lampert, L., 2002. A five channel chlorophyll concentration algorithm applied to SeaWiFS data processed by SeaDAS in coastal waters. *Int. J. Remote Sens.* 23, 1639–1661.
- Gordon, H.R., Morel, A.Y., 1983. Remote assessment of ocean color for interpretation of satellite visible imagery: a review. In: Barber, R.-T., Mooers, C.-N.-K., Bowman, M.-J., Zeitzschel, B. (Eds.), *Lecture notes on coastal and estuarine studies* 4. Springer Verlag, New York.
- Gower, J., King, S., 2007. Validation of chlorophyll fluorescence derived from MERIS on the west coast of Canada. *Int. J. Remote Sens.* 28, 625–635.
- Gower, J., King, S., Borstad, G., Brown, L., 2005. Detection of intense plankton blooms using the 709 nm band of the MERIS imaging spectrometer. *Int. J. Remote Sens.* 26, 2005–2012.
- Grant, M., Jackson, T., Chuprin, A., Sathyendranath, S., Zühlke, M., Storm, T., Boettcher, M., Fomferra, N., 2015. Ocean Colour Climate Change Initiative (OC-CCI) — Phase Two Product User Guide. Issue 2.0.5.

- Gurlin, D., Gitelson, A.A., Moses, W.J., 2011. Remote estimation of Chl-a concentration in turbid productive waters — return to a simple two-band NIR-red model? *Remote Sens. Environ.* 115, 3479–3490.
- Holm-Hansen, O., Lorenzen, C.J., Holmes, R.W., Strickland, J.D., 1965. Fluorometric determination of chlorophyll. *J. Conseil.* 30, 3–15.
- Hooker, S.B., Firestone, E.R., Acker, J.G., Campbell, J.W., Blaisdell, J.M., Darzi, M., 1995. SeaWiFS Technical Report Series. Volume 32: Level-3 SeaWiFS Data Products. Spatial and Temporal Binning Algorithms. Technical Memorandum 104566. NASA Goddard Space Flight Center, Greenbelt, Maryland, USA.
- Hu, C., Lee, Z., Franz, B., 2012. Chlorophyll a algorithms for oligotrophic oceans: a novel approach based on three-band reflectance difference. *J. Geophys. Res. Oceans* 117.
- Jackson, T., Sathyendranath, S., Mélin, F., 2017. An improved optical classification scheme for the ocean colour essential climate variable and its applications. *Remote Sens. Environ.* 203, 152–161.
- Kahru, M., Mitchell, B.G., 2010. Blending of ocean colour algorithms applied to the Southern Ocean. *Remote Sens. Lett.* 1, 119–124.
- Knap, A., Michaels, A., Close, A., Ducklow, H., Dickson, A., 1996. Protocols for the Joint Global Ocean Flux Study (JGOFS) Core Measurements. JGOFS, Reprint of the IOC Manuals and Guides No. 29. 19 UNESCO 1994.
- Le, C., Hu, C., Cannizzaro, J., English, D., Muller-Karger, F., Lee, Z., 2013. Evaluation of chlorophyll-a remote sensing algorithms for an optically complex estuary. *Remote Sens. Environ.* 129, 75–89.
- Le, C., Li, Y., Zha, Y., Sun, D., Huang, C., Zhang, H., 2011. Remote estimation of chlorophyll a in optically complex waters based on optical classification. *Remote Sens. Environ.* 115, 725–737.
- Leathers, R.A., Downes, T.V., Mobley, C.D., 2001. Self-shading correction for upwelling sea-surface radiance measurements made with buoyed instruments. *Opt. Express* 8, 561–570.
- Machu, E., Ferret, B., Garçon, V., 1999. Phytoplankton pigment distribution from SeaWiFS data in the subtropical convergence zone south of Africa: a wavelet analysis. *Geophys. Res. Lett.* 26, 1469. <http://dx.doi.org/10.1029/1999GL900256>.
- Marrari, M., Hu, C., Daly, K., 2006. Validation of SeaWiFS chlorophyll a concentrations in the Southern Ocean: a revisit. *Remote Sens. Environ.* 105, 367–375.
- Matsushita, B., Yang, W., Yu, G., Oyama, Y., Yoshimura, K., Fukushima, T., 2015. A hybrid algorithm for estimating the chlorophyll-a concentration across different trophic states in Asian inland waters. *ISPRS J. Photogramm. Remote Sens.* 102, 28–37.
- Matthews, M.W., Bernard, S., Robertson, L., 2012. An algorithm for detecting trophic status (chlorophyll-a), cyanobacterial-dominance, surface scums and floating vegetation in inland and coastal waters. *Remote Sens. Environ.* 124, 637–652.
- McKee, D., Cunningham, A., Dudek, A., 2007. Optical water type discrimination and tuning remote sensing band-ratio algorithms: application to retrieval of chlorophyll and *k* d (490) in the Irish and Celtic Seas. *Estuar. Coast. Shelf Sci.* 73, 827–834.
- Mishra, S., Mishra, D.R., 2012. Normalized difference chlorophyll index: a novel model for remote estimation of chlorophyll-a concentration in turbid productive waters. *Remote Sens. Environ.* 117, 394–406.
- Mobley, C., Sundman, L., 2008. Hydrolight 5 Ecological 5 Technical Documentation. 98005. Sequoia Scientific, Incorporated, Bellevue, WA, pp. 95.
- Mobley, C.D., 2011. Fast light calculations for ocean ecosystem and inverse models. *Opt. Express* 19, 18927–18944.
- Moore, G., Lavender, S., 2011. Case IIS bright pixel atmospheric correction. MERIS ATBD. 2.
- Moore, T.S., Campbell, J.W., Feng, H., 2001. A fuzzy logic classification scheme for selecting and blending satellite ocean color algorithms. *IEEE Trans. Geosci. Remote Sens.* 39, 1764–1776. <http://ieeexplore.ieee.org/lpdocs/epic03/wrapper.htm?arnumber=942555><http://dx.doi.org/10.1109/36.942555>.
- Moore, T.S., Dowell, M.D., Bradt, S., Verdu, A.R., 2014. An optical water type framework for selecting and blending retrievals from bio-optical algorithms in lakes and coastal waters. *Remote Sens. Environ.* 143, 97–111. <http://www.ncbi.nlm.nih.gov/pubmed/24839311><http://dx.doi.org/10.1016/j.jrse.2013.11.021>.
- Morel, A., Antoine, D., 2011. MERIS ATBD 2.9. Pigment Index Retrieval in Case 1 Waters. Issue 4, Revision 3.
- Morel, A., Prieur, L., 1977. Analysis of variations in ocean color. *Limnol. Oceanogr.* 22, 709–722.
- Moses, W.J., Gitelson, A., Berdnikov, S., Povazhnyy, V., 2009a. Satellite estimation of chlorophyll-concentration using the red and NIR bands of MERIS — the Azov Sea case study. *IEEE Geosci. Remote Sens. Lett.* 6, 845–849.
- Moses, W.J., Gitelson, A.A., Berdnikov, S., Povazhnyy, V., 2009b. Estimation of chlorophyll-a concentration in case II waters using MODIS and MERIS data — successes and challenges. *Environ. Res. Lett.* 4, 045005. <http://stacks.iop.org/1748-9326/4/i=4/a=045005?key=crossref.c3c6caf8da1186e3f3db4700ff27de0><http://dx.doi.org/10.1088/1748-9326/4/4/045005>.
- Mueller, R., Bidigare, R., Trees, C., Balch, W., Dore, J., Drapeau, D., Karl, D., Van Heukelem, L., Perl, J., 2003. Biogeochemical and bio-optical measurements and data analysis protocols: ocean optics protocols for satellite ocean color sensor validation. Revision 5, Vol. V. NASA/TM-2003. pp. 15–26.
- Odermatt, D., Gitelson, A., Brando, V.E., Schaeppman, M., 2012. Review of constituent retrieval in optically deep and complex waters from satellite imagery. *Remote Sens. Environ.* 118, 116–126.
- O'Reilly, J.E., Maritorena, S., Mitchell, B.G., Siegel, D.A., Carder, K.L., Garver, S.A., Kahru, M., McClain, C., 1998. Ocean color chlorophyll algorithms for SeaWiFS. *J. Geophys. Res. Oceans* 103, 24937–24953.
- O'Reilly, J.E., Maritorena, S., Siegel, D.A., O'Brien, M.C., Toole, D., Mitchell, B.G., Kahru, M., Chavez, F.P., Strutton, P., Cota, G.F., et al., 2000. Ocean color chlorophyll a algorithms for SeaWiFS, OC2, and OC4: Version 4. SeaWiFS postlaunch calibration and validation analyses, Part 3, 9–23.
- Pitcher, G., Calder, D., 2000. Harmful algal blooms of the southern Benguela Current: a review and appraisal of monitoring from 1989 to 1997. *S. Afr. J. Mar. Sci.* 22, 255–271.
- Pitcher, G.C., Nelson, G., 2006. Characteristics of the surface boundary layer important to the development of red tide on the southern Namaqua Shelf of the Benguela upwelling system. *Limnol. Oceanogr.* 51, 2660–2674.
- Pitcher, G.C., Weeks, S.J., 2006. The variability and potential for prediction of harmful algal blooms in the southern Benguela ecosystem. *Large Mar. Ecosyst.* 14, 125–146.
- Probyn, T., Pitcher, G., Monteiro, P., Boyd, A., Nelson, G., 2000. Physical processes contributing to harmful algal blooms in Saldanha Bay, South Africa. *S. Afr. J. Mar. Sci.* 22, 285–297.
- Qin, P., Simis, S.G., Tilstone, G.H., 2017. Radiometric validation of atmospheric correction for MERIS in the Baltic Sea based on continuous observations from ships and Aeronet-OC. *Remote Sens. Environ.* 200, 263–280.
- Robertson, L., Bernard, S., Evers-King, H., 2014. Biophysical modelling of phytoplankton communities from first principles using two-layered spheres: Equivalent Algal Populations (EAP) model. *Opt. Express* 22, 16745–16758.
- Roesler, C., Uitz, J., Claustre, H., Boss, E., Xing, X., Organelli, E., Briggs, N., Bricaud, A., Schmechtig, C., Poteau, A., et al., 2017. Recommendations for obtaining unbiased chlorophyll estimates from in situ chlorophyll fluorometers: a global analysis of wet labs eco sensors. *Limnol. Oceanogr. Methods* 15, 572–585.
- Ryan, J.P., Fischer, A.M., Kudela, R.M., Gower, J.F., King, S.A., Marin, R., Chavez, F.P., 2009. Influences of upwelling and downwelling winds on red tide bloom dynamics in Monterey Bay, California. *Cont. Shelf Res.* 29, 785–795.
- Shen, F., Zhou, Y.-X., Li, D.-J., Zhu, W.-J., Suhyb Salama, M., 2010. Medium resolution imaging spectrometer (MERIS) estimation of chlorophyll-a concentration in the turbid sediment-laden waters of the Changjiang (Yangtze) Estuary. *Int. J. Remote Sens.* 31, 4635–4650.
- Shi, K., Li, Y., Li, L., Lu, H., Song, K., Liu, Z., Xu, Y., Li, Z., 2013. Remote chlorophyll-a estimates for inland waters based on a cluster-based classification. *Sci. Total Environ.* 444, 1–15.
- Silió-Calzada, A., Bricaud, A., Gentili, B., 2008. Estimates of sea surface nitrate concentrations from sea surface temperature and chlorophyll concentration in upwelling areas: a case study for the Benguela system. *Remote Sens. Environ.* 112, 3173–3180. <http://dx.doi.org/10.1016/j.jrse.2008.03.014>.
- Siswanto, E., Tang, J., Yamaguchi, H., Ahn, Y.-H., Ishizaka, J., Yoo, S., Kim, S.-W., Kiyomoto, Y., Yamada, K., Chiang, C., et al., 2011. Empirical ocean-color algorithms to retrieve chlorophyll-a, total suspended matter, and colored dissolved organic matter absorption coefficient in the Yellow and East China Seas. *J. Oceanogr.* 67, 627.
- Smith, M.E., Bernard, S., O'Donoghue, S., 2013, Oct, Oct. The assessment of optimal MERIS ocean colour products in the shelf waters of the KwaZulu-Natal Bight, South Africa. *Remote Sens. Environ.* 137, 124–138. <http://linkinghub.elsevier.com/retrieve/pii/S0034425713002022><http://dx.doi.org/10.1016/j.jrse.2013.06.009>.
- Steinmetz, F., Deschamps, P.-Y., Ramon, D., 2011. Atmospheric correction in presence of sun glint: application to MERIS. *Opt. Express* 19, 9783–9800.
- Sun, D., Hu, C., Qiu, Z., Cannizzaro, J.P., Barnes, B.B., 2014. Influence of a red band-based water classification approach on chlorophyll algorithms for optically complex estuaries. *Remote Sens. Environ.* 155, 289–302.
- Trees, C.C., Kennicutt I.I., M.C., Brooks, J.M., 1985. Errors associated with the standard fluorimetric determination of chlorophylls and phaeopigments. *Mar. Chem.* 17, 1–12.
- Vilas, L.G., Spyros, E., Palenzuela, J.M.T., 2011. Neural network estimation of chlorophyll a from MERIS full resolution data for the coastal waters of Galician Rias (NW Spain). *Remote Sens. Environ.* 115, 524–535.
- Vollenweider, R., Kerekes, J., 1982. Eutrophication of waters. monitoring, assessment and control. Organization for Economic Co-operation and Development (OECD).
- Volpe, G., Santoleri, R., Vellucci, V., d'Alcalá, M.R., Marullo, S., d'Ortenzio, F., 2007. The colour of the Mediterranean Sea: global versus regional bio-optical algorithms evaluation and implication for satellite chlorophyll estimates. *Remote Sens. Environ.* 107, 625–638.
- Weeks, S., Barlow, R., Roy, C., Shillington, F., 2006. Remotely sensed variability of temperature and chlorophyll in the southern Benguela: upwelling frequency and phytoplankton response. *Afr. J. Mar. Sci.* 28, 493–509. <http://dx.doi.org/10.2989/18142320609504201>.
- Werdell, P.J., Bailey, S.W., 2005. An improved in-situ bio-optical data set for ocean color algorithm development and satellite data product validation. *Remote Sens. Environ.* 98, 122–140.
- Yacobi, Y.Z., Moses, W.J., Kaganovsky, S., Sulimani, B., Leavitt, B.C., Gitelson, A.A., 2011. NIR-red reflectance-based algorithms for chlorophyll-a estimation in mesotrophic inland and coastal waters: Lake Kinneret case study. *Water Res.* 45, 2428–2436.
- Zibordi, G., Ruddick, K., Ansko, I., Moore, G., Kratzer, S., Icely, J., Reinart, A., 2012. In situ determination of the remote sensing reflectance: an inter-comparison. *Ocean Sci.* 8, 567–586.
- Zibordi, G., Voss, K.J., 2010. Field radiometry and ocean color remote sensing. In: *Oceanography from Space*. Springer, pp. 307–334.